High-Performance Low-Complexity Multi-Sensing-Parameter Association in Perceptive Mobile Networks

Hou-Yu Zhai, Shaoshi Yang, *Senior Member, IEEE*, Xiao-Yang Wang, Jing-Sheng Tan, Yu-Song Luo, and Sheng Chen, *Life Fellow, IEEE*

***Abstract*—The integrated sensing and communication (ISAC) technology has emerged as an enabler that promises to transform the traditional mobile communication networks into the multi-functional perceptive mobile networks (PMNs), where precise positioning and motion state estimation of network nodes can be achieved relying on wireless communications within the network itself. However, in a practical PMN, multiple types of individually estimated parameters corresponding to multiple sensing targets are not naturally associated with each specific target, which may cause severe obstacles to subsequent signal processing tasks, such as positioning and motion state estimation. To address this challenge, a high-performance low-complexity sensing parameter association algorithm is proposed in this paper. Different from previous works, we first develop a novel spatial filter by exploiting the convolutional beamspace based beamformer to separate paths with different directions of arrival (DOA), and then leverage a low-complexity correlation-based algorithm to associate the DOA estimates with the corresponding paired range-velocity estimates. Extensive simulation results are provided to validate the superior performance of the proposed parameter association algorithm over state-of-the-art schemes.**

***Index Terms*—Parameter association, integrated sensing and communication (ISAC), convolutional beamspace (CBS), spatial filtering.**

THE growing demand for environment-aware intelligent mobile networks has driven the concept of perceptive mobile networks (PMNs) [1], which enable high-precision sensing by exploiting wireless communication signals. In general, PMNs primarily utilize two distinct sensing modalities: passive sensing and active sensing. In passive sensing, the base station (BS) estimates the desired sensing parameters by exploiting the reflected signals from user terminals (UTs) or neighboring BSs. Active sensing requires BSs to transmit dedicated signals and process their reflections. High-performance joint communication and active sensing critically depends on full-duplex technology, and it is not sufficiently mature for efficient implementation [1]. Therefore, passive sensing constitutes a competitive alternative.

However, significant challenges also remain for realizing passive sensing in practical PMNs, particularly in the association of multiple types of individually estimated parameters to their corresponding sensing targets. In passive sensing, multiple sensing parameters, such as direction of arrival (DOA), range and velocity, are typically estimated independently. This decoupling creates a critical association problem: the lack of cross-correlation among parameters may result in mismatch among distinct perceived targets. For instance, the velocity estimate of one object could erroneously match with the DOA of another, which may cause severe obstacles to subsequent signal processing tasks, such as positioning and motion state estimation.

To mitigate the impact of parameter mismatch in practical PMNs, the estimates of multi-type sensing parameters of the same perceived target must be identified and associated with each other [2]–[5]. Specifically, the authors of [2] advocated to associate the individual DOA estimates with different UTs by exploiting UT-specific pseudo-random sequences based correlation operation in active sensing. However, this approach cannot be extended to passive sensing scenarios. In [3], DOAs were estimated by exploiting the time-spatial domain measurements, and hence the DOA estimates and range estimates can be naturally associated. Nevertheless, some DOAs may be missing when the ranges of different UTs are close to each other. The mirrored multiple signal classification framework proposed in [4] can mitigate this problem, but its efficacy is primarily restricted to line-of-sight scenarios. In [5], we developed an association algorithm and its low-complexity versions. Specifically, a spatial filter is first utilized to reserve the signals with desired DOAs, then the optimal association with the paired range-velocity estimates is determined by invoking a domain transformation technique. Nevertheless, the computational complexity of the method in [5] is high due to the domain transformation and its reduced-complexity versions exhibit marginal precision degradation.

To overcome the drawbacks of the state-of-the-art solutions conceived for the above-mentioned challenges, in this paper we present a high-performance low-complexity sensing parameter association algorithm. Specifically, we first develop a novel spatial filter to separate paths with different DOAs by

This work was financially supported by Beijing Municipal Natural Science Foundation under Grant L242013.

H.-Y. Zhai, S. Yang (Corresponding author), J.-S. Tan and Y.-S. Luo are with the School of Information and Communication Engineering, Beijing University of Posts and Telecommunications, and the Key Laboratory of Universal Wireless Communications, Ministry of Education, Beijing 100876, China (e-mails: {2hy, shaoshi.yang, jingsheng.tan, yusong.luo}@bupt.edu.cn).

X.-Y Wang is with the Department of Wireless and Terminal Technology, China Mobile Research Institute, Beijing 100053, China (e-mail: wangxiaoyangyjy@chinamobile.com)

S. Chen is with the School of Electronics and Computer Science, University of Southampton, Southampton SO17 1BJ, UK (e-mail: sqc@ecs.soton.ac.uk).

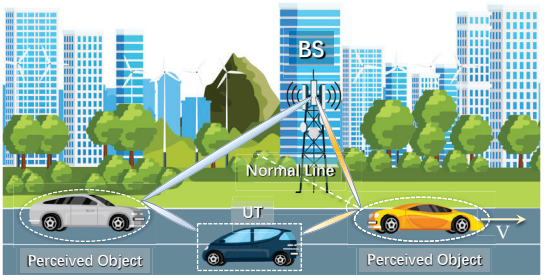

Fig. 1. PMN system model, where the BS achieves passive sensing by exploiting the reflected signals of the vehicular UT.

exploiting the convolutional beamspace (CBS)-based beamformer. Then, we propose a low-complexity correlation-based algorithm to associate DOA estimates with the corresponding paired range-velocity estimates. Finally, extensive simulation results are provided to validate the superior performance of the proposed algorithm.

Notations: $\mathbf{A}^{\mathrm{T}}, \mathbf{A}^{*}, \mathbf{A}^{\mathrm{H}}$ and $\mathbf{A}^{-1}$ represent transpose, conjugate, conjugate transpose and inverse of matrix $\mathbf{A}$, respectively. $\mathbf{a}[i]$ and $\mathbf{A}[i,j]$ denote the ith element of vector $\mathbf{a}$ and the (i,j)th element of $\mathbf{A}$, respectively. $\mathrm{diag}(\mathbf{a}_1,\cdots,\mathbf{a}_n)$ is a block diagonal matrix whose diagonal blocks are $\{\mathbf{a}_1,\cdots,\mathbf{a}_n\}$. $\mathbf{I}_N$ and $\mathbf{0}_{M\times N}$ are the $N\times N$ identity matrix and $M\times N$ zero matrix, respectively. Finally, $*$ is the convolution operator and $\delta(\cdot)$ denotes the Dirac delta function.

I. System Model

We consider a PMN relying on the mmWave band and the multi-input multi-output (MIMO) aided orthogonal frequency division multiplexing (OFDM) technique. As illustrated in Fig. 1, a vehicular UT participates in the wireless communication with distributed BS, and L_{V} vehicles serve as the targets of wireless sensing. For the distributed BS, its baseband unit is connected via the fronthaul to an the remote radio unit (RRU), which is equipped with an M_{R}-element uniform linear array (ULA). The vehicular UT is also equipped with an M_{T}-element ULA. We assume that in addition to the function of wireless communication, the BS can perform sensing by utilizing the signals transmitted from the vehicular UT.

Due to the sparsity of the mmWave channel, only a small number of resolvable propagation paths, denoted by L, exist between the vehicular UT and the RRU [6]. Let the propagation delay and the Doppler offset corresponding to the lth path be τ_l and $f_{\mathrm{D},l}$. By estimating $\{\tau_l\}_{l=1}^{L}$ and $\{f_{\mathrm{D},l}\}_{l=1}^{L}$, the BS achieves both ranging and velocity measurement. The time-domain channel impulse response (CIR) matrix of the uplink from the vehicular UT to the RRU is given by

$$\mathbf{H}(t)=\sum_{l=1}^{L} h_l\delta((1-2v_l/c)t-\tau_l])\mathbf{a}_{M_{\mathrm{R}}}^{\mathrm{T}}(\omega_l)\mathbf{a}_{M_{\mathrm{T}}}(\psi_l), \quad (1)$$

where $\mathbf{a}_{M_{\mathrm{R}}}(\omega_l)=[1,\cdots,e^{j(M_{\mathrm{R}}-1)\omega_l}]\in\mathbb{C}^{1\times M_{\mathrm{R}}}$ and $\mathbf{a}_{M_{\mathrm{T}}}(\psi_l)=[1,\cdots,e^{j(M_{\mathrm{T}}-1)\psi_l}]\in\mathbb{C}^{1\times M_{\mathrm{T}}}$ represent the receiving and transmitting steering vectors of the lth path, respectively, $\omega_l \triangleq \frac{2\pi}{\lambda}d\sin\phi_l$ and $\psi_l\triangleq\frac{2\pi}{\lambda}d\sin\theta_l$ can be interpreted as the spatial frequency corresponding to the incident angles, respectively, while d, λ and c denote the antenna-element spacing, the signal wavelength and the speed of light, respectively. In addition, h_l, v_l, ϕ_l and θ_l represent the channel gain, the velocity of the reflector projected onto the normal direction, the DOA and the angle-of-departure of the signal traveling along the lth path.

As descried in [7], we utilize the data payload for sensing the target vehicles. Let the carrier frequency and the subcarrier spacing be f_{c} and Δf. Furthermore, N_{c} OFDM subcarriers are employed in the system, and $D_n\in\mathbb{C}$ is the modulated data symbol on the nth subcarrier. Therefore, we can represent the signal transmitted by the vehicular UT as

$$\mathbf{x}(t)=\bar{\boldsymbol{\omega}}e^{j2\pi f_{\mathrm{c}}t}\sum_{n=0}^{N_{\mathrm{c}}-1}D_n e^{j2\pi n\Delta f t}, \quad (2)$$

without considering cyclic prefix (CP), where $\bar{\boldsymbol{\omega}}\in\mathbb{C}^{M_{\mathrm{T}}\times 1}$ is the beamforming vector of the vehicular UT. The received baseband signal vector of the gth OFDM symbol $\mathbf{y}_g(t)=e^{-j2\pi f_{\mathrm{c}}t}\mathbf{H}(t)*\mathbf{x}(t)+\mathbf{z}_g(t)$ can be formulated as

$$\begin{aligned}\mathbf{y}_g(t)=&\sum_{l=1}^{L}\sum_{n=0}^{N_{\mathrm{c}}-1}h_l D_n\mathbf{a}_{M_{\mathrm{R}}}^{\mathrm{T}}(\omega_l)\mathbf{a}_{M_{\mathrm{T}}}(\psi_l)\bar{\boldsymbol{\omega}}\\&\times e^{-j2\pi(f_{\mathrm{c}}+n\Delta f)\left(\frac{2v_l}{c}t+(g-1)T_{\mathrm{sym}}+\tau_l\right)}e^{j2\pi n\Delta f t}+\mathbf{z}_g(t), \quad (3)\end{aligned}$$

where $\mathbf{z}_g(t)\in\mathbb{C}^{M_{\mathrm{R}}\times 1}$ is the complex additive white Gaussian noise (AWGN) vector with zero-mean and covariance matrix $\sigma^2\mathbf{I}$. Let the sampling interval, the length of the CP, and the length of an entire OFDM symbol (with CP) be T_{sam}, $T_{\mathrm{cp}}=N_{\mathrm{cp}}T_{\mathrm{sam}}$ and $T_{\mathrm{sym}}=N_{\mathrm{sym}}T_{\mathrm{sam}}$, respectively. Then, the mth sample of the digitized $\mathbf{y}_g[m]\in\mathbb{C}^{M_{\mathrm{R}}\times 1}$ including the impact of CP is formulated as

$$\begin{aligned}\mathbf{y}_g[m]=&\sum_{l=1}^{L}\sum_{n=0}^{N_{\mathrm{c}}-1}e^{-j2\pi f_{\mathrm{c}}\left(\frac{2v_l}{c}(mT_{\mathrm{sam}}+(g-1)T_{\mathrm{sym}}+T_{\mathrm{cp}})+\tau_l\right)}\\&\times e^{-j2\pi n\Delta f\frac{2v_l}{c}(mT_{\mathrm{sam}}+(g-1)T_{\mathrm{sym}}+T_{\mathrm{cp}})}e^{-j2\pi n\Delta f\tau_l}\\&\times e^{j2\pi n\Delta f mT_{\mathrm{sam}}}h_l D_n\mathbf{a}_{M_{\mathrm{R}}}^{\mathrm{T}}(\omega_l)\mathbf{a}_{M_{\mathrm{T}}}(\psi_l)\bar{\boldsymbol{\omega}}+\mathbf{z}_g[m]. \quad (4)\end{aligned}$$

Since $(N_{\mathrm{c}}-1)\Delta f\frac{2v_l}{c}(mT_{\mathrm{sam}}+(g-1)T_{\mathrm{sym}}+T_{\mathrm{cp}})$ is always small, $e^{-j2\pi n\Delta f\frac{2v_l}{c}(mT_{\mathrm{sam}}+(g-1)T_{\mathrm{sym}}+T_{\mathrm{cp}})}$ can be approximated by 1 [8]. Similarly, the term $e^{-j2\pi f_{\mathrm{c}}\left(\frac{2v_l}{c}(mT_{\mathrm{sam}}+(g-1)T_{\mathrm{sym}}+T_{\mathrm{cp}})\right)}$ can be approximated by $e^{-j2\pi f_{\mathrm{c}}\left(\frac{2v_l}{c}((g-1)T_{\mathrm{sym}}+T_{\mathrm{cp}})\right)}$.

Then, the gth received OFDM symbol $\mathbf{Y}_g\in\mathbb{C}^{M_{\mathrm{R}}\times N_{\mathrm{c}}}=[\mathbf{y}_g[0],\mathbf{y}_g[1],\cdots,\mathbf{y}_g[N_{\mathrm{c}}-1]]$ can be expressed as

$$\begin{aligned}\mathbf{Y}_g=&\sum_{l=1}^{L}e^{-j2\pi f_{\mathrm{c}}\left(\frac{2v_l}{c}((g-1)T_{\mathrm{sym}}+T_{\mathrm{cp}})\right)}e^{-j2\pi f_{\mathrm{c}}\tau_l}\\&\times h_l\mathbf{a}_{M_{\mathrm{R}}}^{\mathrm{T}}(\omega_l)\mathbf{a}_{M_{\mathrm{T}}}(\psi_l)\bar{\boldsymbol{\omega}}\boldsymbol{\tau}_l\mathbf{D}\mathbf{F}_{N_{\mathrm{c}}}+\mathbf{Z}_g, \quad (5)\end{aligned}$$

where $\boldsymbol{\tau}_l=[1,\cdots,e^{-j2\pi(N_{\mathrm{c}}-1)\Delta f\tau_l}]\in\mathbb{C}^{1\times N_{\mathrm{c}}}$, $\mathbf{D}=\mathrm{diag}(D_0,\cdots,D_{N_{\mathrm{c}}-1})\in\mathbb{C}^{N_{\mathrm{c}}\times N_{\mathrm{c}}}$, and $\mathbf{F}_{N_{\mathrm{c}}}$ represents the N_{c}-dimension inverse fast Fourier transform (IFFT) matrix, while $\mathbf{Z}_g=[\mathbf{z}_g[0],\mathbf{z}_g[1],\cdots,\mathbf{z}_g[N_{\mathrm{c}}-1]]\in\mathbb{C}^{M_{\mathrm{R}}\times N_{\mathrm{c}}}$.

To further estimate propagation delay $\{\tau_l\}_{l=1}^{L}$ and Doppler offset $\{f_{\mathrm{D},l}\}_{l=1}^{L}$, a common method is to firstly compensate the received signal by exploiting the demodulated communication data as $\overline{\mathbf{Y}}_g=\mathbf{Y}_g\mathbf{F}^{\mathrm{H}}\mathbf{D}^{-1}$, which is also exploited in

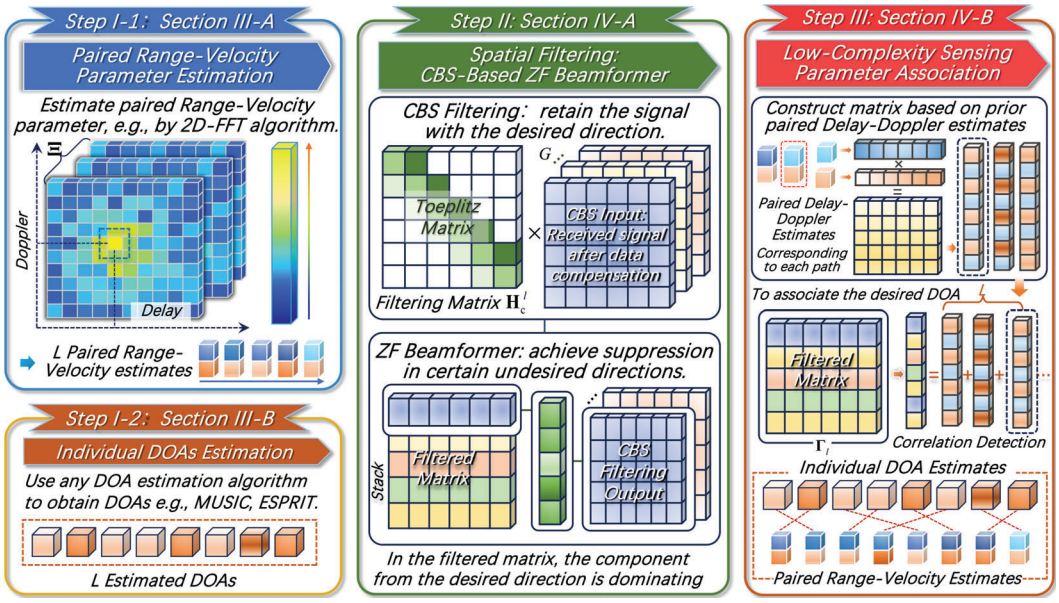

Fig. 2. Framework of the proposed sensing parameter association algorithm. In *Step I*, the BS achieves passive sensing, after which the paired range-velocity estimates and individual DOA estimates are obtained. In *Step II*, to associate DOA $\hat{\phi}_l$, the spatial filtering is applied to suppress the interference signals from other undesired directions. Finally, in *Step III*, we achieve the association of the individual DOA estimates with the paired range-velocity estimates.

[8].

To overcome the drawbacks of existing solutions, we propose a novel sensing parameter association framework as depicted in Fig. 2, which is detailed as follows. Specifically, Section II elaborates *Step I* of achieving the sensing parameter estimation, while Section III presents both the proposed spatial filtering for suppressing the interference signals (*Step II*) and the proposed association scheme (*Step III*).

II. Uplink Sensing Problem Formulation

Step I of Fig. 2 illustrates how we achieve passive sensing in OFDM-based PMNs. Specifically, a two-dimensional fast Fourier transform (2D-FFT) is firstly applied to obtain the paired Delay-Doppler estimation (*Step I-1*), and the individual DOA estimates are then obtained (*Step I-2*).

A. Paired Delay-Doppler Estimation

Let $\overline{\mathbf{y}}_{g,m}\in\mathbb{C}^{1\times N_c}$ be the mth row of $\overline{\mathbf{Y}}_g$, and define $\mathbf{\Gamma}_m=\left[(\overline{\mathbf{y}}_{1,m})^{\mathrm{T}},\cdots,(\overline{\mathbf{y}}_{G,m})^{\mathrm{T}}\right]^{\mathrm{T}}\in\mathbb{C}^{G\times N_c}$. Then we have

$$\mathbf{\Gamma}_m=\sum\nolimits_{l=1}^{L}\alpha_{l,m}\boldsymbol{\theta}_l\boldsymbol{\tau}_l+\overline{\mathbf{W}}_m, \tag{6}$$

where $\alpha_{l,m}=e^{-j2\pi f_c\tau_l}h_l\mathbf{a}_{M_R}^{\mathrm{T}}(\omega_l)[m]\mathbf{a}_{M_T}(\psi_l)\bar{\boldsymbol{\omega}}$, $\boldsymbol{\theta}_l=\left[e^{-j2\pi f_c\frac{2v_l}{c}T_{\mathrm{cp}}},\cdots,e^{-j2\pi f_c\frac{2v_l}{c}[(G-1)T_{\mathrm{sym}}+T_{\mathrm{cp}}]}\right]^{\mathrm{T}}\in\mathbb{C}^{G\times 1}$, and $\overline{\mathbf{W}}_m$ is a complex AWGN matrix. To improve the sensing resolution, the zero-padding technique is employed to expand the dimension of $\mathbf{\Gamma}_m$. Let $\mathbf{\Gamma}_{K,m}$ be the zero-padding-version of $\mathbf{\Gamma}_m$, which is given by

$$\mathbf{\Gamma}_{K,m}=\begin{bmatrix}\mathbf{\Gamma}_m & \mathbf{0}_{G\times(K-1)N_c}\\ \mathbf{0}_{(K-1)G\times N_c} & \mathbf{0}_{(K-1)G\times(K-1)N_c}\end{bmatrix}, \tag{7}$$

where K is the multiple of zero-padding length, indicating the dimension scaling of $\mathbf{\Gamma}_{K,m}$ relative to $\mathbf{\Gamma}_m$. Then, the output of the 2D-FFT of $\mathbf{\Gamma}_{K,m}$, $\mathbf{\Xi}=\mathbf{F}_{KG}^{*}\mathbf{\Gamma}_{K,m}\mathbf{F}_{KNc}^{*}\in\mathbb{C}^{KG\times KN_c}$ can be expressed as

$$\mathbf{\Xi}=\sum\nolimits_{l=1}^{L}\alpha_{l,m}\left(\mathbf{F}_{KG}^{*}\bar{\boldsymbol{\theta}}_{K,l}\right)\left(\mathbf{F}_{KN_c}^{\mathrm{H}}\bar{\boldsymbol{\tau}}_{K,l}^{\mathrm{T}}\right)^{\mathrm{T}}+\tilde{\mathbf{W}}_{K,m}, \tag{8}$$

where $\bar{\boldsymbol{\theta}}_{K,l}=\left[\boldsymbol{\theta}_l^{\mathrm{T}},\mathbf{0}_{1\times(K-1)G}\right]^{\mathrm{T}}\in\mathbb{C}^{KG\times 1}$, $\bar{\boldsymbol{\tau}}_{K,l}=\left[\boldsymbol{\tau}_l,\mathbf{0}_{1\times(K-1)N_c}\right]\in\mathbb{C}^{1\times KN_c}$, and $\tilde{\mathbf{W}}_{K,m}=\mathbf{F}_{KG}^{*}\overline{\mathbf{W}}_{K,m}\mathbf{F}_{KN_c}^{*}$ is the AWGN matrix.

Define $\boldsymbol{\gamma}_{l,G}=\left(\mathbf{F}_{KG}^{*}\bar{\boldsymbol{\theta}}_{K,l}\right)\in\mathbb{C}^{KG\times 1}$ and $\boldsymbol{\gamma}_{l,N_c}^{\mathrm{T}}=\left(\mathbf{F}_{KN_c}^{\mathrm{H}}\bar{\boldsymbol{\tau}}_{K,l}^{\mathrm{T}}\right)^{\mathrm{T}}\in\mathbb{C}^{1\times N_c}$. Thus, $\boldsymbol{\gamma}_{l,G}$ and $\boldsymbol{\gamma}_{l,N_c}^{\mathrm{T}}$ can be expressed as the discrete Fourier transform (DFT) samples of $\bar{\boldsymbol{\theta}}_{K,l}$ and $\bar{\boldsymbol{\tau}}_{K,l}^{\mathrm{T}}$, respectively. Let the Fourier transform (FT) of the finite-sequence $\bar{\boldsymbol{\theta}}_{K,l}$ be $\bar{\boldsymbol{\gamma}}_{l,G}(f)$, i.e.,

$$\bar{\boldsymbol{\gamma}}_{l,G}(f)=\sum\nolimits_{g=0}^{KG-1}\bar{\boldsymbol{\theta}}_{K,l}[g]e^{-j2\pi fg}. \tag{9}$$

Similarly, let the FT of the finite-sequence $\bar{\boldsymbol{\tau}}_{K,l}^{\mathrm{T}}$ be $\bar{\boldsymbol{\gamma}}_{l,N_c}(f)$. To associate the DFT samples with the continuous FT, the resolution of $\boldsymbol{\gamma}_{l,G}$ and $\boldsymbol{\gamma}_{l,N_c}$ have to be determined. According to [8], the sampling intervals F_{R} and T_{R} for $\boldsymbol{\gamma}_{l,G}$ and $\boldsymbol{\gamma}_{l,N_c}$ are the reciprocal of the total time period and that of the entire bandwidth, namely, $F_{\mathrm{R}}=1/(KGT_{\mathrm{sym}})$ and $T_{\mathrm{R}}=1/(KN_c\Delta f)$, respectively. Thus, we have $\boldsymbol{\gamma}_{l,G}[i]=\bar{\boldsymbol{\gamma}}_{l,G}(iF_{\mathrm{R}})=\bar{\boldsymbol{\gamma}}_{l,G}(\frac{i\Delta f}{KG})$ and $\boldsymbol{\gamma}_{l,N_c}[p]=\bar{\boldsymbol{\gamma}}_{l,N_c}(pT_{\mathrm{R}})=\bar{\boldsymbol{\gamma}}_{l,N_c}(\frac{pT_{\mathrm{sam}}}{K})$. As a result, the (i,p)th element in $\mathbf{\Xi}$ is

$$\mathbf{\Xi}[i,p]=\sum_{l=1}^{L}2\pi^2\alpha_{l,m}\bar{\boldsymbol{\gamma}}_{l,G}\left(\frac{i\Delta f}{KG}\right)\bar{\boldsymbol{\gamma}}_{l,N_c}^{\mathrm{T}}\left(\frac{pT_{\mathrm{sam}}}{KN_c}\right)+\tilde{\mathbf{W}}_{K,m}[i,p]. \tag{10}$$

According to the definitions of $\boldsymbol{\gamma}_{l,G}$ and $\boldsymbol{\gamma}_{l,N_c}$, it is intuitive that $\mathbf{\Xi}$ is the sum of the Gaussian noises $\tilde{\mathbf{W}}_{K,m}$ and the linear

summation of L discrete 2D sample matrices $\{\boldsymbol{\gamma}_{l,G}\boldsymbol{\gamma}_{l,N_c}^{\mathrm{T}}\}_{l=1}^{L}$. Each 2D sample matrix, $\boldsymbol{\gamma}_{l,G}\boldsymbol{\gamma}_{l,N_c}^{\mathrm{T}}$, corresponds to the signals reflected by an object, and the delay-Doppler peak coordinates $(\hat{\kappa}_l, \hat{\epsilon}_l)$ for the lth component matrix of $\boldsymbol{\Xi}$ satisfy

$$(\hat{\kappa}_l, \hat{\epsilon}_l) = \arg\min_{k,n\in\mathbb{Z}^+} |(k - f_{\mathrm{D},l}/\Delta f) f_{\mathrm{R}}, (n - \tau_l/T_{\mathrm{sam}}) T_{\mathrm{R}}|^2, \quad (11)$$

where $\mathbb{Z}^+$ represents the set of non-negative integers. After determining the coordinates of the peak values $\{(\hat{\kappa}_l, \hat{\epsilon}_l)\}_{l=1}^{L}$, we can obtain the paired range-velocity estimates by $\{\hat{r}_l = \hat{\epsilon}_l R_{\mathrm{u}}\}_{l=1}^{L}$ and $\{\hat{v}_l = \hat{\kappa}_l V_{\mathrm{u}}\}_{l=1}^{L}$, where $R_{\mathrm{u}} = cT_{\mathrm{R}} = c/KN_{\mathrm{sub}}\Delta f$ and $V_{\mathrm{u}} = cf_{\mathrm{R}}/f_{\mathrm{c}} = c/Kf_{\mathrm{c}}T_{\mathrm{sym}}G$ are defined as the range resolution and velocity resolution, respectively.

B. DOA Estimation and Problem Formulation

Various DOA estimation algorithms have been proposed in open literature [12]–[14]. By exploiting any of these algorithms, we can estimate the individual DOAs.

However, since these DOA estimates $\{\hat{\phi}_i\}_{i=1}^{L}$ are generally obtained independently of the range-velocity estimation, it is challenging to associate individual DOA estimates with the paired range-velocity estimates belonging to the same individual targets. In this paper, we aim to properly associate the individual DOA estimates with the paired range-velocity estimates.

III. Sensing Parameter Association

This section establishes the association between DOAs and the corresponding paired range-velocity estimates. First, we develop a novel spatial filter to separate multipath components with distinct DOAs by exploiting the CBS-based zero forcing (ZF) beamformer design. Consequently, component matrices with undesired DOAs are suppressed, while the component matrix with the desired DOA is dominating in the output matrix. Next, as each component matrix in the output matrix corresponds to a specific paired delay-Doppler estimate, we then develop a low-complexity correlation-based association algorithm to determine the optimal DOA mapping to the paired range-velocity estimates. Finally, we obtain L paired range-velocity-DOA sensing parameters $\{(\hat{r}_l, \hat{v}_l, \hat{\phi}_l)\}_{l=1}^{L}$.

A. Spatial Filtering: CBS-Based ZF Beamformer Design

First, the CBS possessing is implemented to retain the signals from desired direction ϕ_l, by convolving $\overline{\mathbf{Y}}_g$ with a spatial domain FIR filter $\{h_{\mathrm{c}}^l(m)\}_{m=1}^{M}$, with M denoting the length of the filter[1]. In fact, the output of the CBS possessing can also be expressed as multiplying the received signal $\overline{\mathbf{Y}}_g$ by a banded Toeplitz matrix $\mathbf{H}_{\mathrm{c}}^l$ [10]. Thus, the output $\mathbf{Y}_{\mathrm{c},g} \in \mathbb{C}^{(M_{\mathrm{R}}-M+1)\times N_{\mathrm{c}}}$ can be expressed as

$$\mathbf{Y}_{\mathrm{c},g} = \mathbf{H}_{\mathrm{c}}^l \overline{\mathbf{Y}}_g = \sum\nolimits_{l=1}^{L} \overline{h}_l \mathbf{H}_{\mathrm{c}}^l \mathbf{a}_{M_{\mathrm{R}}}^{\mathrm{T}}(\omega_l)\mathbf{a}_{M_{\mathrm{T}}}(\psi_l)\boldsymbol{\omega}\bar{\boldsymbol{\tau}}_l + \mathbf{Z}_{\mathrm{c},g}, \quad (12)$$

where $\overline{h}_l \in \mathbb{C} = h_l e^{-j2\pi f_{\mathrm{c}}\left(\frac{2v_l}{c}((g-1)T_{\mathrm{sym}}+T_{\mathrm{cp}})\right)} e^{-j2\pi f_{\mathrm{c}}\tau_l}$, and $\mathbf{H}_{\mathrm{c}}^l \in \mathbb{C}^{(M_{\mathrm{R}}-M+1)\times M_{\mathrm{R}}}$ is a banded Toeplitz matrix:

$$\mathbf{H}_{\mathrm{c}}^l = \begin{bmatrix} h_{\mathrm{c}}^l(M-1) & \cdots & h_{\mathrm{c}}^l(0) & 0 & \cdots & 0 \\ 0 & h_{\mathrm{c}}^l(M-1) & \cdots & h_{\mathrm{c}}^l(0) & \cdots & 0 \\ \vdots & \vdots & \vdots & \vdots & \ddots & \vdots \\ 0 & 0 & \cdots & h_{\mathrm{c}}^l(M-1) & \cdots & h_{\mathrm{c}}^l(0) \end{bmatrix}. \quad (13)$$

The output $\mathbf{Y}_{\mathrm{c},g}$ in (12) can be further expanded as

$$\mathbf{Y}_{\mathrm{c},g} = \sum_{l=1}^{L} \underbrace{\overline{h}_l e^{j(M-1)\omega_l} H_{\mathrm{c}}^l(\omega_l)\mathbf{a}_{M_{\mathrm{R}}-M+1}^{\mathrm{T}}(\omega_l)\mathbf{a}_{M_{\mathrm{T}}}(\psi_l)\bar{\boldsymbol{\omega}}\boldsymbol{\tau}_l}_{\text{the signal component from } l\text{th path, with DOA } \phi_l} + \mathbf{Z}_{\mathrm{c},g}, \quad (14)$$

where $H_{\mathrm{c}}^l(\omega) = \sum_{m=0}^{M-1} h_{\mathrm{c}}^l(m) e^{-j\omega m}$ denotes the spatial frequency response of the filter $\{h_{\mathrm{c}}^l(m)\}_{m=1}^{M}$, and $\mathbf{a}_{M_{\mathrm{R}}-M+1}(\omega_l)$ contains the first $(M_{\mathrm{R}}-M+1)$ elements of the array steering vector $\mathbf{a}_{M_{\mathrm{R}}}(\omega_l)$. By CBS processing, all the arriving signals are filtered by the response $H_{\mathrm{c}}^l(\omega)$. Ideally, the signal from the desired direction ϕ_l should be perfectly retained, and all the signals from undesired directions should be suppressed.

Next, to achieve enhanced suppression of interference signals from undesired directions, we design the beamformer vector $\mathbf{v}_l \in \mathbb{C}^{1\times(M_{\mathrm{R}}-M+1)}$. We mainly consider to cancel the interference signals from undesired directions $\{\phi_k\}_{k=1,k\neq l}^{L}$, while maximizing the beam gain over the desired direction ϕ_l. The following optimization problem is considered:

$$\max_{\mathbf{v}_l} \ G_{\mathbf{v}_l}(\phi_l) = |\mathbf{v}_l \mathbf{a}_{M_{\mathrm{R}}-M+1}^{\mathrm{T}}(\omega_l)|^2, \quad (15a)$$

$$\text{s.t.} \ \ \|\mathbf{v}_l\|_2^2 = 1, G_{\mathbf{v}_l}(\phi_k) = 0, \ k = 1, \cdots, L, k \neq l, \quad (15b)$$

Then, the tight upper bound of the full array gain over the desired direction ϕ_l in (15a) is $\overline{G}_{\mathbf{v}_l}(\phi_l) \leq \|\mathbf{v}_l\|^2 \left\|\mathbf{a}_{M_{\mathrm{R}}-M+1}^{\mathrm{T}}(\omega_l)\right\|^2 = M_{\mathrm{R}} - M + 1$. According to [11], the optimal solution for maximizing $G_{\mathbf{v}_l}(\phi_l)$ under the null-steering constraint is given by the ZF beamformer:

$$\mathbf{v}_l^{\mathrm{ZF}} = \frac{[\mathbf{I}_{M_{\mathrm{R}}-M+1} - \mathbf{A}(\mathbf{A}^{\mathrm{H}}\mathbf{A})^{-1}\mathbf{A}^{\mathrm{H}}]\mathbf{a}_{M_{\mathrm{R}}-M+1}(\phi_l)}{\|[\mathbf{I}_{M_{\mathrm{R}}-M+1} - \mathbf{A}(\mathbf{A}^{\mathrm{H}}\mathbf{A})^{-1}\mathbf{A}^{\mathrm{H}}]\mathbf{a}_{M_{\mathrm{R}}-M+1}(\phi_l)\|_2}, \quad (16)$$

with $\mathbf{A} = [\mathbf{a}_{M_{\mathrm{R}}-M+1}(\omega_1), \cdots, \mathbf{a}_{M_{\mathrm{R}}-M+1}(\omega_k), \cdots, \mathbf{a}_{M_{\mathrm{R}}-M+1}(\omega_L)] \in \mathbb{C}^{(M_{\mathrm{R}}-M+1)\times(L-1)}$.

Then, we stack the filtered signals $\{\mathbf{v}_l^{\mathrm{ZF}}\mathbf{Y}_{\mathrm{c},g}\}_{g=1}^{G}$ into $\boldsymbol{\Gamma}^l$ as $[(\mathbf{v}_l^{\mathrm{ZF}}\mathbf{Y}_{\mathrm{c},1})^{\mathrm{T}}, \cdots, (\mathbf{v}_l^{\mathrm{ZF}}\mathbf{Y}_{\mathrm{c},G})^{\mathrm{T}}]^{\mathrm{T}}$. Specifically, there establishes

$$\boldsymbol{\Gamma}_l = \sum_{l=1}^{L} \beta_l(\omega_l)\boldsymbol{\Xi}_l + \breve{\mathbf{Z}} = \underbrace{\beta_l(\omega_l)\boldsymbol{\theta}_l\boldsymbol{\tau}_l}_{} + \underbrace{\sum\nolimits_{k\neq l}^{L} \beta_k(\omega_k)\boldsymbol{\theta}_k\boldsymbol{\tau}_k}_{} + \breve{\mathbf{Z}}, \quad (17)$$

where $\boldsymbol{\Xi}_l \in \mathbb{C}^{G\times N_{\mathrm{c}}} = \boldsymbol{\theta}_l\boldsymbol{\tau}_l$ for $l = 1, \cdots, L$, and $\beta_l(\omega_l) \in \mathbb{C} = e^{-j2\pi f_{\mathrm{c}}\tau_l} h_l e^{j(M-1)\omega_l} H_{\mathrm{c}}^l(\omega_l)\mathbf{v}_l^{\mathrm{ZF}}\mathbf{a}_{M_{\mathrm{R}}-M+1}^{\mathrm{T}}(\omega_l)\ \mathbf{a}_{M_{\mathrm{T}}}(\psi_l)\boldsymbol{\omega}$.

Thus, $\boldsymbol{\Gamma}_l$ can be regarded as the spatial-filtered-version $\boldsymbol{\Gamma}_m$: the component $\boldsymbol{\Xi}_l$ from desired direction ϕ_l is dominating in (17), while other components $\{\boldsymbol{\Xi}_k\}_{k\neq l}^{L}$ from undesired directions $\{\phi_k\}_{k\neq l}^{L}$ are suppressed.

[1] Actually, there have been numerous methods to design a digital FIR filter. In this paper, we only consider the basic window method to generate a band-pass FIR filter, which is given by $h_{\mathrm{c}}^l(m) = \sin[\omega_{\mathrm{H}}(m-M_L)]/\pi(m-M_L) - \sin[\omega_{\mathrm{L}}(m-M_L)]/\pi(m-M_L)$ for $m = 1, \cdots, M_L$, where $M_L = (M-1)/2$, ω_{H} and ω_{L} denote the high and low cut-off frequencies, respectively.

Algorithm 1 Sensing Parameter Association

Input: $\{(\hat{\kappa}_l, \hat{\epsilon}_l)\}_{l=1}^{L}$, $\{\hat{\phi}_l\}_{l=1}^{L}$, $\{\overline{\mathbf{Y}}_g\}_{g=1}^{G}$, $\{\mathbf{H}_{\mathrm{c}}^{l}\}_{l=1}^{L}$.

1: Construct $\{\hat{\mathbf{\Xi}}_i\}_{i=1}^{L}$ by $\{(\hat{\kappa}_l, \hat{\epsilon}_l)\}_{l=1}^{L}$.
2: **for** $l=1$ to L **do**
3: Obtain $\{\mathbf{Y}_{\mathrm{c},g}\}_{g=1}^{G}$ and $\mathbf{v}_l^{\mathrm{ZF}}$ by (12) and (16), respectively.
4: Obtain $\mathbf{\Gamma}_l$ by stacking the filtered signals $\{\mathbf{v}_l^{\mathrm{ZF}}\mathbf{Y}_{\mathrm{c},g}\}_{g=1}^{G}$.
5: Determine the optimal association index b_l for $\hat{\phi}_l$ by (19).
6: Associate DOA estimates $\hat{\phi}_l$ with the paired Delay-Doppler estimates $(\hat{\kappa}_{b_l}, \hat{\epsilon}_{b_l})$.
7: **end for**

Output: The associated parameters: $(\hat{r}_i, \hat{v}_i, \hat{\phi}_i)$, $i = 1, \cdots, L$.

B. Low-Complexity Sensing Parameter Association

Since each matrix $\hat{\mathbf{\Xi}}_l$ corresponds to a specific paired delay-Doppler estimate $(\hat{\kappa}_l, \hat{\epsilon}_l)$, we can construct matrices $\{\hat{\mathbf{\Xi}}_l\}_{l=1}^{L}$ by the prior estimates $\{(\hat{\kappa}_l, \hat{\epsilon}_l)\}_{l=1}^{L}$. Specifically, the (m,n)th element of $\hat{\mathbf{\Xi}}_l$ is denoted as

$$\hat{\mathbf{\Xi}}_l[m,n] = e^{-j2\pi\left(f_{\mathrm{c}}\frac{2\hat{v}_l}{c}[(m-1)T_{\mathrm{sym}}+T_{\mathrm{cp}}]+(n-1)\Delta f\hat{\epsilon}_l\right)}. \quad (18)$$

Note that the components matrices $\{\mathbf{\Xi}_k\}_{k=1,k\neq l}^{L}$ from undesired directions $\{\phi_k\}_{k=1,k\neq l}^{L}$ in (17) have been suppressed, we just need to identify which component matrix in $\mathbf{\Gamma}_l = \sum_{l=1}^{L=1}\beta_l(\omega_l)\mathbf{\Xi}_l + \breve{\mathbf{Z}}$ has the largest contribution, thus realizing the association of $\hat{\phi}_l$ with $(\hat{\kappa}_l, \hat{\epsilon}_l)$, and in turn, with $(\hat{r}_l, \hat{v}_l)$.

Before proceeding to the specific solution process, we first demonstrate the linear independence of matrices $\{\hat{\mathbf{\Xi}}_l\}_{l=1}^{L}$ to ensure the decomposition uniqueness of the noise-free $\mathbf{\Gamma}_l$.

Theorem 1: *For $l \in \{1, 2, \cdots, L\}$, all the component matrices $\{\hat{\mathbf{\Xi}}_i\}_{i=1}^{L}$ in $\mathbf{\Gamma}_l$ are linearly independent when $\hat{\kappa}_1 \neq \hat{\kappa}_2 \neq \cdots \neq \hat{\kappa}_L$ or/and $\hat{\epsilon}_1 \neq \hat{\epsilon}_2 \neq \cdots \neq \hat{\epsilon}_L$.*

The proof is omitted due to the page limit.

The linear independence proved in **Theorem 1** ensures that the contributions of $\{\hat{\mathbf{\Xi}}_l\}_{l=1}^{L}$ in $\mathbf{\Gamma}_l$ are non-overlapping and statistically distinguishable. Then, to achieve the association for $\hat{\phi}_l$ for any given $l \in \{1, \cdots, L\}$, we just need to identify which matrix component offers the maximum contribution in $\mathbf{\Gamma}_l$. Specifically, by defining $b_l \in \{1, \cdots, L\}$ as the optimal association index between $\hat{\phi}_l$ and $\{\hat{\mathbf{\Xi}}_l\}_{l=1}^{L}$, we have:

$$b_l = \arg\max_{i\in\{1,\cdots,L\}} \langle \mathbf{\Gamma}_l, \hat{\mathbf{\Xi}}_i\rangle / \|\mathbf{\Gamma}_l\|_{\mathrm{F}} \cdot \|\hat{\mathbf{\Xi}}_i\|_{\mathrm{F}}. \quad (19)$$

It is intuitive that $\langle \mathbf{\Gamma}_l, \hat{\mathbf{\Xi}}_i\rangle / \|\mathbf{\Gamma}_l\|_{\mathrm{F}}\|\hat{\mathbf{\Xi}}_i\|_{\mathrm{F}}$ is maximized when $i = l$. On the contrary, if $i \neq l$, $\langle \mathbf{\Gamma}_l, \hat{\mathbf{\Xi}}_i\rangle / \|\mathbf{\Gamma}_l\|_{\mathrm{F}}\|\hat{\mathbf{\Xi}}_i\|_{\mathrm{F}}$ will be much smaller since the contribution of $\hat{\mathbf{\Xi}}_i$ in $\mathbf{\Gamma}_l$ is negligible. Thus, $\hat{\phi}_l$ is associated with $\hat{\mathbf{\Xi}}_l$ by (19), and in turn with the paired delay-Doppler estimate $(\hat{\kappa}_l, \hat{\epsilon}_l)$.

Consequently, we can obtain L paired range-velocity-DOA sensing parameters $\{(\hat{r}_l, \hat{v}_l, \hat{\phi}_l)\}_{l=1}^{L}$. Table III-A summarizes the proposed sensing parameter association procedure.

C. Complexity Analysis

The computational complexity of the full association algorithm in [5] is $\mathcal{O}(4G^2M_{\mathrm{R}}N_{\mathrm{c}}L + 2G^2N_{\mathrm{c}}L + 2GN_{\mathrm{c}}^2L)$. Upon considering the same spatial filter, the computational complexity of the proposed parameter association scheme is $\mathcal{O}(LGN_{\mathrm{c}} + L^2GN_{\mathrm{c}})$. In addition, the complexity of the proposed CBS-based ZF spatial filter is roughly $\mathcal{O}((L-1)^2(M_{\mathrm{R}} - M + 1) + (L-1)^3)$.

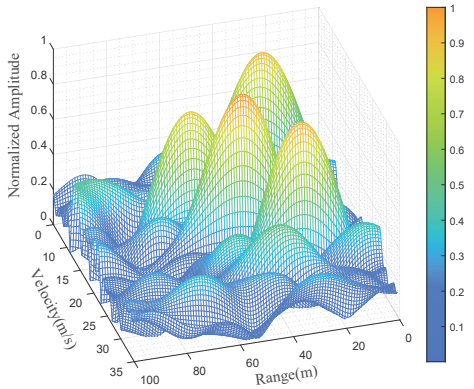

Fig. 3. An implementation of (10) and the paired delay-Doppler estimates can be obtained by locating all the peaks of $|\mathbf{\Xi}|$.

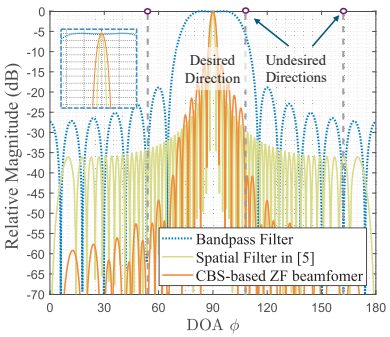

Fig. 4. Beampatterns of different spatial filters, where we set the desired direction and undesired directions to 0.5π and $\{0.3\pi, 0.6\pi, 0.9\pi\}$.

IV. Numerical Results

In the simulations, the numbers of BS and UT antennas are set to $M_{\mathrm{R}} = 64$ and $M_{\mathrm{T}} = 2$, respectively. The carrier frequency is set to $f_{\mathrm{c}} = 28\,\mathrm{GHz}$ and the subcarrier spacing is set to 100 KHz [4]. Furthermore, the number of subcarriers is chosen to be 128 and the length of CP is 16. In each simulation trial, three perceived targets are randomly generated in the range of $[20,\ 90]$ m, whose velocities are randomly generated in the range of $[0,\ 40]$ m/s. The DOAs of the perceived targets are randomly sampled from $[0, \pi]$. In Fig. 3, we illustrate a realization of $|\mathbf{\Xi}|$ and the $K = 25$ times zero-padding technique is utilized to improve sensing resolution. By locating all the peaks of $|\mathbf{\Xi}|$, we can obtain the desired paired delay-Doppler estimates, and the corresponding range-velocity estimates.

First, we evaluate the spatial filtering performance, which is depicted in Fig. 4. Specifically, the equivalent beampatterns of different spatial filters are illustrated, where the filter length is set to $M = 31$ and the passband of the spatial FIR filter is defined as $\phi \in [0.4\pi,\ 0.6\pi]$. Compared to the spatial filter proposed in [5] (based on ULA with $M_{\mathrm{R}} = 64$), the proposed CBS-based ZF beamformer has an approximate main lobe

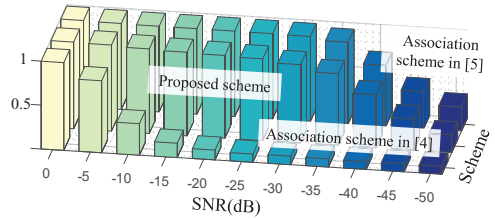

Fig. 5. The probability of success association of the proposed scheme and the association methods described in [4], [5].

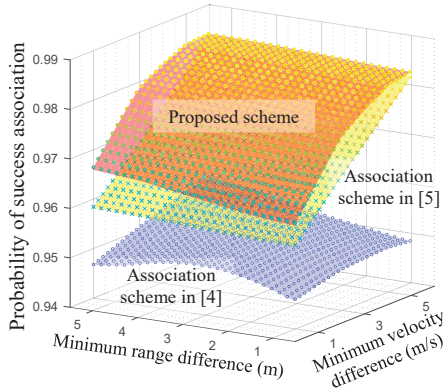

Fig. 6. The probability of success association of the proposed scheme and the association methods described in [4], [5].

width. However, it sacrifices approximately 4 to 5 dB of side-lobe performance while providing significantly enhanced suppression performance over a wider angular range. Furthermore, the ZF design in the proposed scheme enables substantial suppression in certain undesired directions.

Then, we evaluate the average probabilities of success association by different association schemes under low signal-to-noise ratio (SNR) conditions in Fig. 5. In this scenario, five perceived targets are considered and each result is derived from 10^3 independent Monte Carlo trials. Specifically, the proposed association algorithm achieves nearly the identical performance to the scheme in [5], while the complexity of our algorithm is significantly reduced. Notably, the association performance of the scheme in [4] exhibits substantial fluctuations as SNR decreases, whereas both our scheme and the scheme in [5] maintain robust performance even at extremely low SNRs.

In Fig. 6, we evaluate the robustness of the three schemes in a more comprehensive manner. Specifically, we introduce two configurable parameters: the minimum differences among velocities and ranges of perceived targets, namely $\Delta r_{\min} = \min_{i \neq j} |r_i - r_j|$ and $\Delta v_{\min} = \min_{i \neq j} |v_i - v_j|$. This setup is designed to emulate challenging scenarios, such as those with multiple closely-spaced perceived targets. When these targets have similar kinematic states, the ambiguity in sensing parameter association increases. The velocity and location of each perceived target are randomly generated to ensure generality and each result in Fig. 6 is derived from 500 independent Monte Carlo trials. As depicted in Fig. 6, for our scheme and the schemes of [4], [5], the probabilities of success slightly decrease as the minimum differences in velocity and range are reduced. Notably, even in the scenarios with the lowest success probability, our scheme consistently outperforms the other two schemes.

V. Conclusion

To implement a more practical range-velocity-DOA sensing in PMNs, we propose a high-performance low-complexity sensing parameter association algorithm. Specifically, we develop a novel spatial filter to separate paths with distinct DOAs by exploiting the CBS-based beamformer design. Then, we propose a low-complexity correlation-based algorithm to associate DOA estimates with the corresponding paired range-velocity estimates, without the need for complicated domain transformation. Extensive simulation results are provided, validating the superior performance of the proposed algorithm. The effectiveness of the proposed method relies on distinct path DOAs, and its resolution performance for closely spaced targets can be limited. Future work will involve developing spatial filtering techniques of higher robustness for dense environments.

References

[1] F. Dong, *et al.*, "Sensing as a service in 6G perceptive mobile networks: Architecture, advances, and the road ahead," *IEEE Network*, vol. 38, no. 2, pp. 87–96, Mar. 2024.

[2] Z. Ni, *et al.*, "Estimation of multiple angle-of-arrivals with localized hybrid subarrays for millimeter wave systems," *IEEE Transactions on Communications*, vol. 68, no. 3, pp. 1897–1910, Mar. 2020.

[3] S.-F. Chuang, W.-R. Wu, and Y.-T. Liu, "High-resolution AoA estimation for hybrid antenna arrays," *IEEE Transactions on Antennas and Propagation*, vol. 63, no. 7, pp. 2955–2968, Jul. 2015.

[4] Z. Ni, *et al.*, "Uplink sensing in perceptive mobile networks with asynchronous transceivers," *IEEE Transactions on Signal Processing*, vol. 69, pp. 1287–1300, Feb. 2021.

[5] X.-Y. Wang, *et al.*, "Clutter suppression, time-frequency synchronization, and sensing parameter association in asynchronous perceptive vehicular networks," *IEEE Journal on Selected Areas in Communications*, vol. 42, no. 10, pp. 2719–2736, Oct. 2024.

[6] R.-W. Heath, *et al.*, "An overview of signal processing techniques for millimeter wave MIMO systems," *IEEE Journal of Selected Topics in Signal Processing*, vol. 10, no. 3, pp. 436–453, Apr. 2016.

[7] J. A. Zhang, *et al.*, "Enabling joint communication and radar sensing in mobile networks–A survey," *IEEE Communications Surveys & Tutorials*, vol. 24, no. 1, pp. 306–345, 2022.

[8] Y. Liu, *et al.*, "Super-resolution range and velocity estimations with OFDM integrated radar and communications waveform," *IEEE Transactions on Vehicular Technology*, vol. 69, no. 10, pp. 11659–11672, Oct. 2020.

[9] J. A. Zhang, M. L. Rahman, X. Huang, Y. J. Guo, S. Chen, and R. W. Heath, "Perceptive mobile networks: Cellular networks with radio vision via joint communication and radar sensing," *IEEE Vehicular Technology Magazine*, vol. 16, no. 2, pp. 20–30, Jun. 2021.

[10] P. -C. Chen and P. P. Vaidyanathan, "Convolutional beamspace for linear arrays," *IEEE Transactions on Signal Processing*, vol. 68, pp. 5395–5410, Sep. 2020.

[11] Z. Xiao, L. Zhu, L. Bai, and X.-G. Xia, *Array Beamforming Enabled Wireless Communications,* Boca Raton, Florida, USA: CRC Press, 2023.

[12] R. Schmidt, "Multiple emitter location and signal parameter estimation," *IEEE Transactions on Antennas and Propagation*, vol. 34, no. 3, pp. 276–280, Mar. 1986.

[13] R. Roy and T. Kailath, "ESPRIT-estimation of signal parameters via rotational invariance techniques," *IEEE Transactions on Acoustics, Speech, and Signal Processing*, vol. 37, no. 7, pp. 984–995, Jul. 1989.

[14] A. Hu, T. Lv, H. Gao, Z. Zhang, and S. Yang, "An ESPRIT-based approach for 2-D localization of incoherently distributed sources in massive MIMO systems," *IEEE Journal of Selected Topics in Signal Processing*, vol. 8, no. 5, pp. 996–1011, Oct. 2014.